ADVANCED FUNCTIONAL MATERIALS
www.afm-journal.de

Composition Engineering of All-Inorganic Perovskite Film for Efficient and Operationally Stable Solar Cells

Jingjing Tian, Jing Wang, Qifan Xue, Tianqi Niu, Lei Yan, Zonglong Zhu, Ning Li,* Christoph J. Brabec, Hin-Lap Yip,* and Yong Cao*

Cesium-based inorganic perovskites have recently attracted great research focus due to their excellent optoelectronic properties and thermal stability. However, the operational instability of all-inorganic perovskites is still a main hindrance for the commercialization. Herein, a facile approach is reported to simultaneously enhance both the efficiency and long-term stability for all-inorganic $CsPbI_{2.5}Br_{0.5}$ perovskite solar cells via inducing excess lead iodide (PbI_2) into the precursors. Comprehensive film and device characterizations are conducted to study the influences of excess PbI_2 on the crystal quality, passivation effect, charge dynamics, and photovoltaic performance. It is found that excess PbI_2 improves the crystallization process, producing high-quality $CsPbI_{2.5}Br_{0.5}$ films with enlarged grain sizes, enhanced crystal orientation, and unchanged phase composition. The residual PbI_2 at the grain boundaries also provides a passivation effect, which improves the optoelectronic properties and charge collection property in optimized devices, leading to a power conversion efficiency up to 17.1% with a high open-circuit voltage of 1.25 V. More importantly, a remarkable long-term operational stability is also achieved for the optimized $CsPbI_{2.5}Br_{0.5}$ solar cells, with less than 24% degradation drop at the maximum power point under continuous illumination for 420 h.

1. Introduction

Since the first report in 2009,[1] organic–inorganic hybrid perovskite solar cells (PSCs) have attracted tremendous attention due to their superior optoelectronic properties.[2–6] The 10 years' developments have witnessed a huge advancement of PSCs, with certified power conversion efficiency (PCE) increasing from an initial 3.8% up to a record 25.2%,[7] approaching the champion efficiency reported for the best monocrystalline silicon solar cells (27.6%). Despite the impressive progress of PSCs, their device stability remains an inevitable concern for the commercialization. Considering the high volatility of the organic cations (e.g., $CH_3NH_3^+$, MA^+; $CH_3(NH_2)_2^+$, FA^+), organic–inorganic hybrid perovskites generally suffer from the chemical instability, especially at high-temperature environment.[8–10] In this regard, all-inorganic cesium (Cs)-based PSCs, which are more robust under thermal stress, have gained increased research interest. As the inorganic monovalent cation Cs^+ has an ionic radius comparable to those of the organic A-site ions, it can be satisfactorily used to meet the requirements of the formation of robust ABX_3 perovskite structure. Meanwhile, the strong interaction between the inorganic $[BX_6]^{4-}$ framework and Cs^+ also endows the better thermal stability of all-inorganic perovskites, which are stable even up to 300 °C.[11,12]

Among all the inorganic perovskites, α-$CsPbI_3$ (cubic phase) with a desirable bandgap of ≈1.73 eV is suitable for the application in solar cells. However, the α-$CsPbI_3$ phase suffers from the phase instability, which would spontaneously transform from black α-phase into the undesired yellow δ-phase (orthorhombic

J. Tian, Prof. Q. Xue, T. Niu, L. Yan, Prof. H.-L. Yip, Prof. Y. Cao
State Key Laboratory of Luminescent Materials and Devices
Institute of Polymer Optoelectronic Materials and Devices
School of Materials Science and Engineering
South China University of Technology
381 Wushan Road, Guangzhou 510640, P. R. China
E-mail: qfxue@scut.edu.cn; msangusyip@scut.edu.cn

J. Wang, Prof. Z. Zhu
Department of Chemistry
City University of Hong Kong
Tat Chee Avenue, Kowloon, Hong Kong

The ORCID identification number(s) for the author(s) of this article can be found under https://doi.org/10.1002/adfm.202001764.

© 2020 The Authors. Published by WILEY-VCH Verlag GmbH & Co. KGaA, Weinheim. This is an open access article under the terms of the Creative Commons Attribution License, which permits use, distribution and reproduction in any medium, provided the original work is properly cited.

DOI: 10.1002/adfm.202001764

Prof. Q. Xue, Prof. H.-L. Yip
Innovation Center for Printed Photovoltaics
South China Institute of Collaborative Innovation
Dongguan 523808, P. R. China

Dr. N. Li, Prof. C. J. Brabec
Institute of Materials for Electronics and Energy Technology (i-MEET)
Friedrich-Alexander University Erlangen-Nürnberg
Martensstraße 7, Erlangen 91058, Germany
E-mail: ning.li@fau.de

Dr. N. Li, Prof. C. J. Brabec
Helmholtz-Institute Erlangen-Nürnberg (HI ERN)
Forschungszentrum Jülich
Immerwahrstrasse 2, Erlangen 91058, Germany

Dr. N. Li
National Engineering Research Center for Advanced Polymer Processing Technology
Zhengzhou University
Zhengzhou 450002, China

phase) under ambient conditions at room temperature, hindering the long-term application.[13,14] Many efforts have been devoted to stabilizing the α-phase of $CsPbI_3$ for photovoltaic applications, such as crystallization engineering,[15] additive engineering,[16–22] interface engineering,[22–26] compositional optimization,[27–30] dimensional engineering,[31,32] and synthesis of nanocrystals.[33] However, the small Goldschmidt tolerance factor t (≈0.8) of $CsPbI_3$ is the root cause, leading to the unstable cubic lattice structure at room temperature. Instead, $CsPbI_xBr_{3-x}$ mixed halide perovskites, which are formed by partially replacing iodine (2.2 Å) with the smaller bromine halide ion (1.96 Å), could provide much better structural stability, making them as a new research hotspot for perovskite solar cells.[34,35]

Although the $CsPbI_xBr_{3-x}$ perovskites show better thermal and structural stability, their photostability is still a critical issue to be solved. It was reported that under illumination, photoinduced phase segregation of the halide anions could be occurred in the mixed halide all-inorganic perovskites,[36–38] and therefore to better evaluate the overall performance of the PSCs, their operational stability should be studied.[39–41] Several reports revealed that ion migration is initiated by the halide defects at the grain boundaries (GBs) of the polycrystalline perovskite film and eventually results in Br-rich and I-rich perovskite phases.[42–45] Therefore, in order to improve the operational stability of mixed-halide inorganic PSCs, it is urgently needed to improve the film quality and reduce the density of defects. One common strategy used for grain boundary passivation is the introduction of small amount of excess PbI_2 in the perovskite films, which significantly improves the PSC performance.[46–48] Yang and co-workers first reported that passivation of $MAPbI_3$ with PbI_2 could improve the efficiency of PSCs.[46] Seok and co-workers also demonstrated that the incorporation of excess PbI_2 could be beneficial to passivate the trap states of $MAPbI_3$ film. It was claimed that excess PbI_2 could act as a passivation layer between the GBs, affecting defect states, dangling bonds, ion migration, etc.[42] Although excess PbI_2 has been widely considered as an effective trap-state passivation method, its effects on the all-inorganic PSCs was rarely investigated.

Stability test is important for evaluating the overall performance of perovskite solar cells. However, in the literatures, the stability test of PSCs was performed under different conditions, ranging from placing unencapsulated devices in the dark under uncontrolled ambient conditions and periodically measuring their PCE, to studies that were under controlled atmosphere, illumination, temperature, and load.[39] Different experimental conditions influence the ageing behavior considerably, making it difficult to compare these results. Many research groups have investigated the differences in ageing behavior with respect to different conditions and found that ageing at the maximum power point (MPP) represents the closest condition resembling that of a working solar cell. Therefore, using MPP tracking to study the operational stability is the most appropriate and reliable way to report stability of PSCs.[39–41] Here, the effect of excess PbI_2 on device performance and operational stability is systematically investigated by incorporating different amount of PbI_2 into the all-inorganic $CsPbI_{2.5}Br_{0.5}$ perovskite precursor. It is found that the presence of a small amount of excess crystalline PbI_2 in all-inorganic $CsPbI_{2.5}Br_{0.5}$ perovskite has great benefits in improving the overall performance and device stability. The optimized PSCs was achieved by adding 1.02 mmol PbI_2 in the precursor solution, which produces a champion PSC with a PCE of 17.1% and a high V_{OC} of 1.25 V, which is among the highest efficiencies reported for this type of all-inorganic PSCs. In addition, the devices also show excellent operating stability and maintain 76% of their initial efficiency after continuous illumination at the MPP for over 400 h. To the best of our knowledge, this is the first demonstration of operationally stable all-inorganic mixed-halide PSCs. Our results demonstrate that adding moderate amount of PbI_2 in all-inorganic PSCs can induce higher film crystallinity, lower defects density, lower charge recombination, and rapid charge transport, suggesting that such a simple composition engineering strategy can effectively improve both the efficiency and stability of all-inorganic PSCs.

2. Results

We began our research by evaluating the photovoltaic performance of the PbI_2-passivated $CsPbI_{2.5}Br_{0.5}$ PSCs. The perovskite films were deposited by the one-step spin-coating method from the precursor with a recipe of x mmol PbI_2 (x = 1.00, 1.02, 1.04, 1.06), 0.5 mmol CsBr, and 0.5 mmol CsI in a mixture solvent of dimethyl sulfoxide (DMSO) and dimethylformamide (DMF). For ease of description, the films with different amount of PbI_2 are abbreviated as 1.00-PbI_2, 1.02-PbI_2, 1.04-PbI_2, and 1.06-PbI_2. All the devices were fabricated with the planar architecture of indium tin oxide (ITO)/SnO_2/ZnO/perovskite/Spiro-OMeTAD/MoO_3/Ag.

Figure 1a shows the representative current density–voltage (J–V) characteristics of the champion devices based on 1.00-PbI_2 (control) and 1.02-PbI_2 (optimized) perovskite precursors, and the photovoltaic performances are summarized in **Table 1**. The control device shows a relatively low efficiency of 15.2%, with open-circuit voltage (V_{OC}), current density (J_{SC}), and fill factor (FF) of 1.19 V, 16.00 mA cm^{-2}, and 79.2%, respectively. By contrast, the optimized 1.02-PbI_2 device achieves a higher PCE of 17.1%, with V_{OC}, J_{SC}, and FF of 1.25 V, 16.50 mA cm^{-2}, and 82.8%, respectively. The increased PCE of the optimized devices mainly comes from the improvements of V_{OC} and FF. The significantly improved champion PCE with a low V_{OC}-deficits of 0.57 V demonstrates the effectiveness of excess PbI_2 in fabricating high-efficiency all-inorganic PSCs. The J–V characteristics and photovoltaic performances of the PSCs with the different amount of PbI_2 are shown in Figure S1 and Table S1 in the Supporting Information. When the amount of PbI_2 increases to 1.04 and 1.06, the device performance decreases due to the fact that the excess PbI_2 may hinder the charge carrier transport at the GBs. The corresponding external quantum efficiency (EQE) curves are illustrated in Figure 1b. The integrated current density matches well with the J_{SC} values observed from the J–V scan. The higher EQE value at 550–640 nm is attributed to the increased carrier collection efficiency close to the hole transporting layer (HTL)/anode interface and the reduced charge carrier recombination, caused by the smoother and more uniform surface of 1.02-PbI_2 perovskite film (main reason, Figure S2, Supporting

© 2020 The Authors. Published by WILEY-VCH Verlag GmbH & Co. KGaA, Weinheim

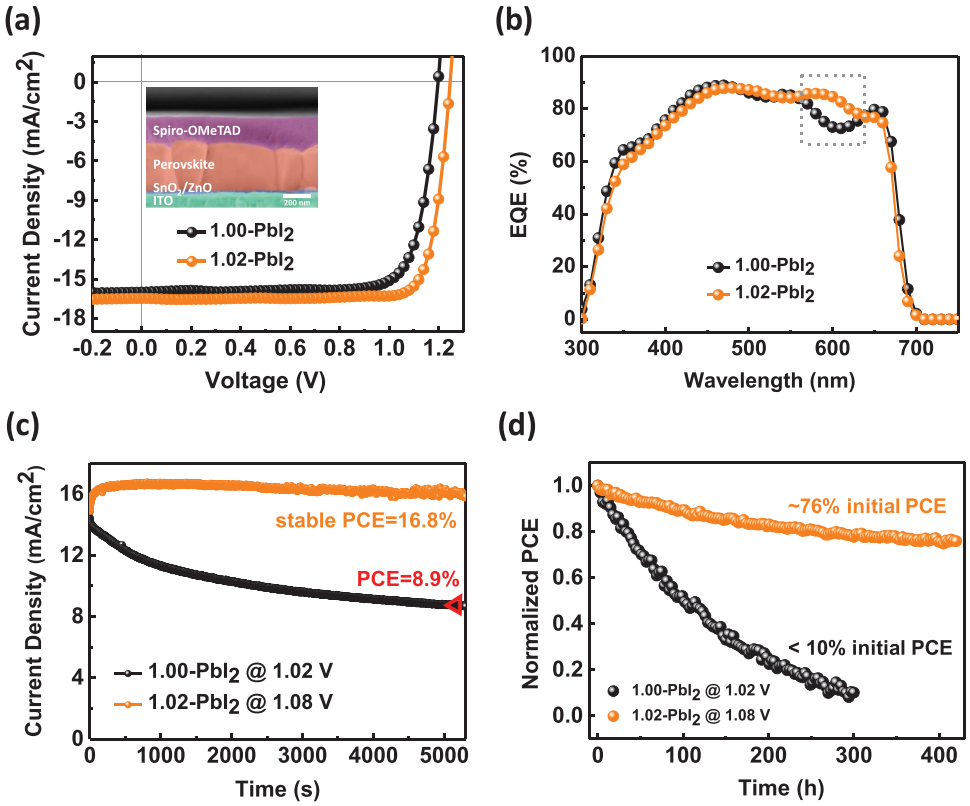

Figure 1. a) *J–V* characteristics and b) EQE spectrum of the champion devices fabricated from 1.00- and 1.02-PbI_2 perovskite precursors. c) The J_{SC} evolution of the devices with 1.00- and 1.02-PbI_2 perovskite films during a continuous operation at the maximum power point under 1 sun conditions. d) Operational stability of the devices with 1.00- and 1.02-PbI_2 perovskite films. The devices are examined at the maximum power point with a constant load (1.02 and 1.08 V for 1.00-PbI_2 and 1.02-PbI_2 devices, respectively) under continuous full-sun, AM 1.5G illumination in glovebox. Under this condition, the continuous power output is monitored in our PSCs.

Information) and the defects passivation of PbI_2 at the GBs.[49] The J_{SC} evolution under 1 sun illumination was further evaluated and depicted in Figure 1c. The 1.02-PbI_2 device presents a better photostability during the test period, whereas the control device shows a fast degradation with time and reduces by over 40% after 90 min illumination. The observation suggests the enhanced trap suppression effect by felicitously introducing the excess PbI_2 in all-inorganic $CsPbI_{2.5}Br_{0.5}$ perovskite. The improved trap-mediated recombination and limited ion migration benefit the stable power output under the long-term operational condition. The improved stability was further testified by the long-term operational stability test, as shown in Figure 1d. The 1.02-PbI_2 device retains 76% of their initial efficiency after continuous power output at the MPP for 420 h with a constant load of 1.08 V (the voltage at the MPP from initial *J–V* curve). While the control device shows a poor operational stability, which loses over 90% of their initial efficiency within 300 h with a constant load of 1.02 V. The lifetime to 80% of the initial value (t_{80}) was extracted from the degradation curves.[50] The detailed quantitative analysis demonstrates a t_{80} lifetime as high as 260 h of 1.02-PbI_2 device, which significantly outperforms the 33 h for control device. The correlated changes in device performances imply that the adding excess PbI_2 is highly effective for synergistically enhancing the PCE and stability of $CsPbI_{2.5}Br_{0.5}$ devices. We attribute the key effect provided by the excess PbI_2 to the formation of extra PbI_2 at the GBs, which efficiently passivates the traps and reduces trap-mediated recombination. In addition, extra PbI_2 also physically limits the ion migration at the GBs and is beneficial to achieve stable power output under the long-term operational condition, which will be discussed thoroughly below.

Table 1. Photovoltaic performance of the champion perovskite devices with 1.00- and 1.02-PbI_2 concentration.

PbI_2 [mmol mL^{-1}]	V_{oc} [V]	J_{sc} [mA cm^{-2}]	FF [%]	PCE [%]
1.00	1.19	16.00	79.21	15.2
1.02	1.25	16.50	82.80	17.1

3. Discussion

To explore the underlying mechanisms of the significant improvements in device efficiency and operational stability of the PbI_2-passivated devices, we first estimated the optical and structural properties of the excess PbI_2-incorporated perovskite films. Figure S3 in the Supporting Information shows the UV–vis absorption spectra of the perovskite films with different amount of PbI_2. All the cases exhibit similar light absorption with a same bandgap (E_g) of 1.82 eV, indicating that the optical

© 2020 The Authors. Published by WILEY-VCH Verlag GmbH & Co. KGaA, Weinheim

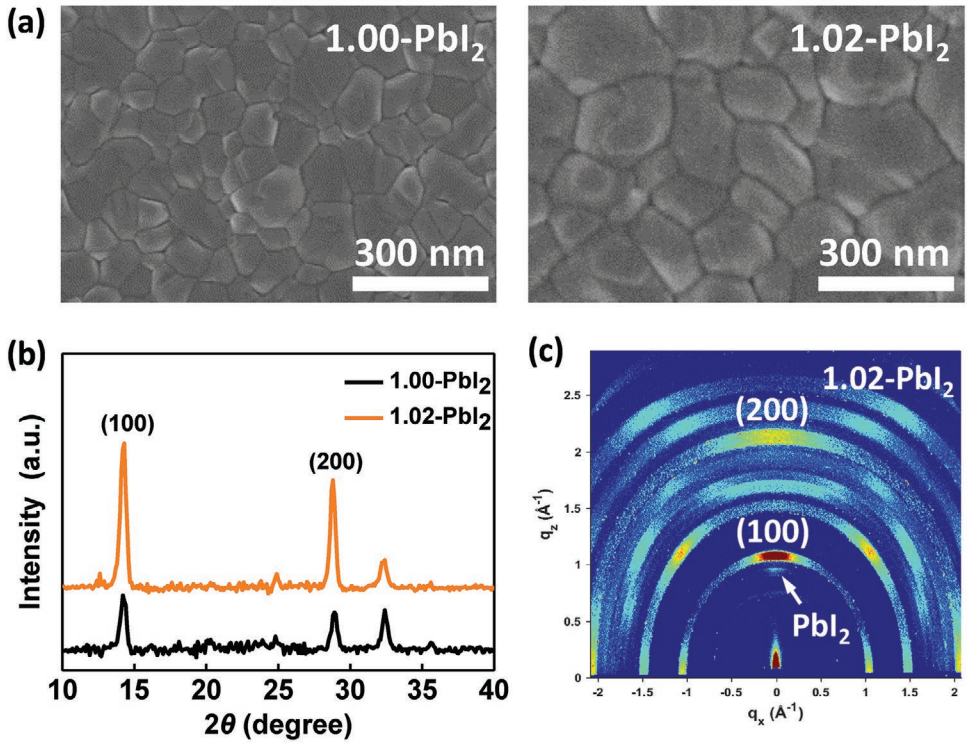

Figure 2. The characterization of the perovskite thin films: a) Plane-view SEM images and b) XRD patterns of different amount of PbI_2 concentration: 1.00-PbI_2 and 1.02-PbI_2. c) 2D grazing-incidence wide-angle X-ray scattering (GIWAXS) image of the film fabricated from "1.02-PbI_2" perovskite precursor.

effect plays negligible role on the final device performance. The plane-view scanning electron microscopy (SEM) images are illustrated for the representative control and optimized 1.02-PbI_2 samples in **Figure 2**a. The 1.02-PbI_2 film exhibits the significantly enlarged grain sizes with fewer GBs with respect to the control film, indicating the positive effects of excess PbI_2 in regulating the crystallization dynamics.[51,52] When the amount of PbI_2 was further increased, 1.04-PbI_2 and 1.06-PbI_2 samples with larger grains showed obvious bright PbI_2 phase on the perovskite surface.[53,54] All PbI_2 phase forms around the perovskite grain boundary on the surface, similar to the previously reported works on organic–inorganic hybrid perovskite solar cells.[42,46,47,55,56] The X-ray diffraction (XRD) patterns are shown in Figure 2b. Both the films present two typical peaks of α-phase $CsPbI_{2.5}Br_{0.5}$ phase located at 14.2° and 28.8° for the (100) and (200) crystal planes, respectively. The unchanged peak positions indicate the excess PbI_2 in precursor has not been incorporated into the perovskite crystal lattice during the film formation, leading to a negligible influence of phase composition. Meanwhile, the strong diffraction peak at 12.6° indicates the coexistence of PbI_2 in 1.02-PbI_2 film. The narrower full width at half maximum of diffraction peaks and corresponding enhanced crystallinity of 1.02-PbI_2 film are in good agreement with the SEM results. The crystal texture was further assessed using grazing incidence wide-angle X-ray scattering (GIWAXS) analysis (Figure S4, Supporting Information, and Figure 2c). Both samples exhibit the similar features of the 3D perovskite structure represented by the broad Debye–Scherrer rings. The intensity versus q_z curve for the scattering features is shown in Figure S5 in the Supporting Information, the increased intensity of diffraction peaks in the 1.02-PbI_2 case indicated that there is more oriented crystal presented in the perovskite film. A small PbI_2 diffraction peak at q_z = 0.935 Å^{-1} observed in PbI_2-excess sample is in accordance with the XRD results. The observations above suggest that the excess PbI_2 doping could effectively influence the crystal nucleation behavior in the precursor solutions and slow down the growth process of perovskite films, which may be due to the promotion of the formation of Lewis base adduct of PbI_2(DMSO) in the precursors.[57] It is well known that PbI_2 could easily combine with DMSO solvent to form PbI_2-DMSO complex.[58,59] Thus, excess PbI_2 forms a larger concentration of PbI_2(DMSO) intermediate phase in the perovskite precursor, retarding the fast reaction between PbI_2, CsI, and CsBr to form $CsPbI_{2.5}Br_{0.5}$ phase during the spin-coating process and then resulting in less crystal nucleus. When annealing the precursor film, the more PbI_2(DMSO) adduct will slow down the crystallization of perovskite and give more time for crystal nucleus growth, inducing the inorganic perovskite grains to grow larger and obtaining the high-quality $CsPbI_{2.5}Br_{0.5}$ films with better orientation. After annealing, the residual PbI_2 located at the GBs is expected to passivate the defects, thus contributes to the improved optoelectronic properties. The enhanced film quality cooperated with the PbI_2-passivation effect benefit the PSCs achieving the long-term operational stability.

The steady-state photoluminescence (PL) and time-resolved PL (TRPL) spectra were carried out to investigate the charge transport property and recombination behavior of the effect

© 2020 The Authors. Published by WILEY-VCH Verlag GmbH & Co. KGaA, Weinheim

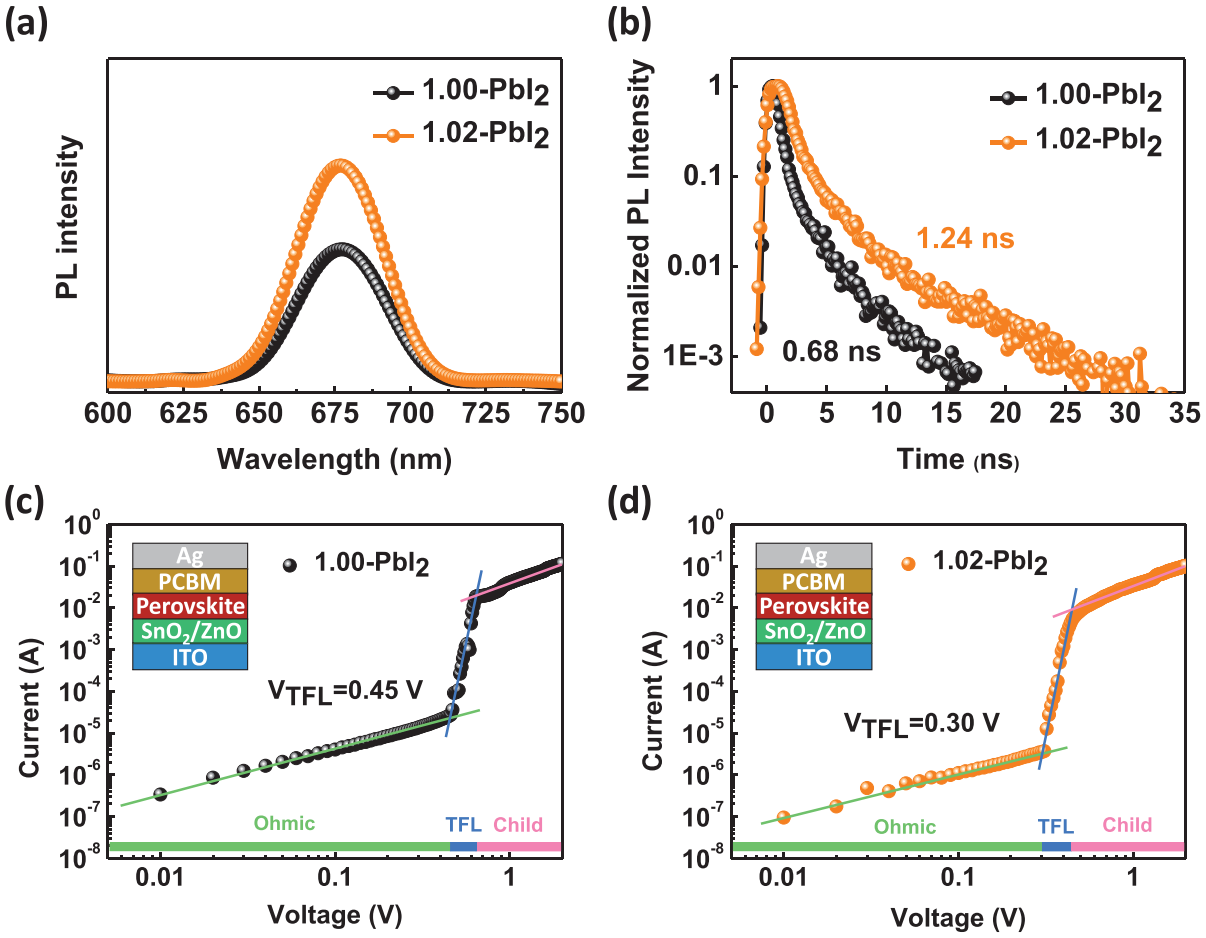

Figure 3. a) Steady state PL and b) time-resolved PL of the perovskite films prepared under 1.00-PbI_2 and 1.02-PbI_2 conditions. c,d) Trap density extraction by dark current–voltage measurement of the electronic-only device, with the device structure of ITO/SnO_2/ZnO/perovskite/PCBM/Ag. The green lines represent the ohmic regime of each case and the sky-blue lines indicate the trap-filled limit (TFL) regime with the onset voltage (V_{TFL}).

of excess PbI_2. As displayed in **Figure 3**a, the 1.02-PbI_2 film exhibits the stronger PL intensity without significant peak shift, indicating the effective suppression of the nonradiative recombination and negligible influence in phase composition of the excess PbI_2 within perovskite films. Through fitting the TRPL curves by single-exponential function, the 1.02-PbI_2 film exhibits the doubled carrier lifetime of 1.24 ns in contrast to 0.68 ns of control film (Figure 3b and Table S2, Supporting Information). The results demonstrate the excess PbI_2 could effectively inhibit the nonradiative recombination and elongated the carrier lifetime in $CsPbI_{2.5}Br_{0.5}$ films.

To further quantitatively study the defect-state density of perovskite films with different amount of PbI_2, we fabricated the electron-only device with structure of ITO/SnO_2/ZnO/perovskite/[6,6]-phenyl-C_{61}-butyric acid methyl ester (PCBM)/Ag and evaluated the defect-state density via the trap-filled limit voltage (V_{TFL}) using Equation (1)

$$N_t = \frac{2\varepsilon_0\varepsilon_r V_{TFL}}{qL^2} \quad (1)$$

where ε_0 is the vacuum permittivity, ε_r is the relative dielectric constant (ε_r = 35),[60,61] V_{TFL} is the onset voltage of the trap-filled limit region, q is the elemental charge, and L is the thickness of the $CsPbI_{2.5}Br_{0.5}$ film (350 nm). From Figure 3c,d, the defect-state density is estimated to be 1.42×10^{16} cm^{-3} and 9.49×10^{15} cm^{-3} for the 1.00-PbI_2 and 1.02-PbI_2 perovskite films, respectively. The results of 1.04-PbI_2 and 1.06-PbI_2 cases are also shown in Figure S6 in the Supporting Information. Among all the cases, a lowest trap density was observed in the 1.02-PbI_2 film. The decrease in defect-state density could be attributed to the enhanced crystallinity and the effective defect passivation of the excess PbI_2 at the GBs. However, the further increased concentration causes the unwished defects around the GBs on the perovskite surface, resulting from the aggregation of the residual PbI_2 observed for samples with 1.04-PbI_2 and 1.06-PbI_2. The lowest trap density in 1.02-PbI_2 perovskite film would promote effective charge transport and suppress the halide ion migration under illumination, which leads to the improvement in efficiency and operational stability of the PSCs.

Combining our characterization results, we speculated that the residual PbI_2 is mainly existed at the GBs, which plays a crucial role in passivating defects and reducing carrier recombination in the absorber films. The mechanism schematic is summarized in **Scheme 1**. Due to the solution-based deposition processes are far from thermodynamic equilibrium, a

© 2020 The Authors. Published by WILEY-VCH Verlag GmbH & Co. KGaA, Weinheim

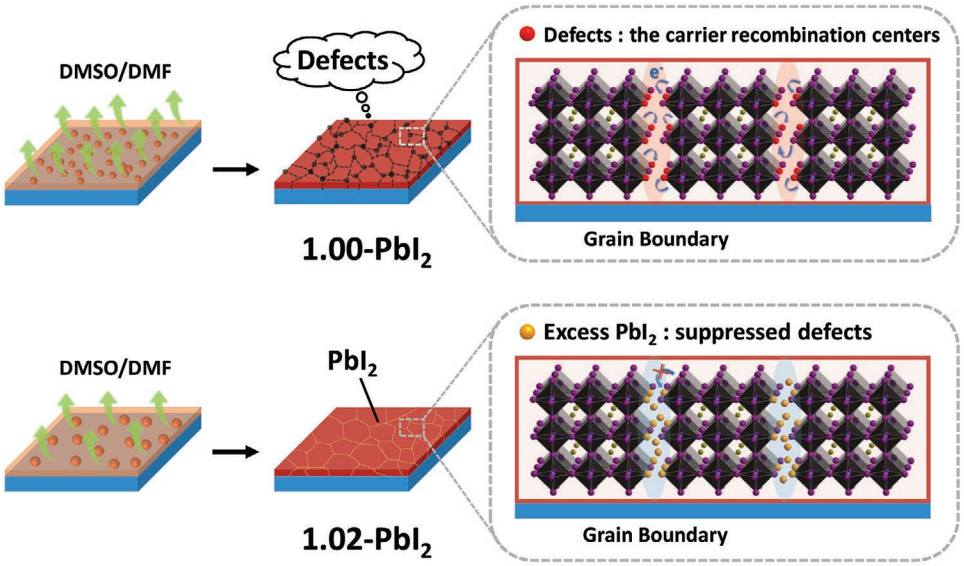

Scheme 1. Proposed mechanism for 1.00- and 1.02-PbI_2 in perovskite film.

large number of defects at the GBs coexist in the polycrystalline $CsPbI_{2.5}Br_{0.5}$ film. These defects acting as undesirable carrier recombination centers would hinder the charge extraction and collection, leading to increase energy loss, and even accelerate the degradation process under external loading condition. By contrast, the slight excess PbI_2 in optimized film could not only improve the nucleation and growth process to obtain the high-quality perovskite film but also serve as the passivator between the adjacent perovskite grains, hindering the charge recombination. It is known that the energy offset between the molecules and perovskite also plays an important role in trap state passivation and intergranular carrier transport.[62] The conduction band minimum (CBM) and the valence band maximum (VBM) for $CsPbI_{2.5}Br_{0.5}$ are −3.48 and −5.30 eV, respectively. And the CBM and VBM for PbI_2 are −3.40 and −5.80 eV, respectively. Therefore, the type I band alignment forms between PbI_2 and $CsPbI_{2.5}Br_{0.5}$ perovskite (Figures S7 and S8, Supporting Information). PbI_2 is well known as a p-type semiconductor with a large bandgap. The n–p junction should thus form at the $CsPbI_{2.5}Br_{0.5}$-PbI_2 interface when excess p-type PbI_2 is introduced. From the energy band structure, the VBM of p-type PbI_2 has a disparity of 0.5 eV with the VBM of $CsPbI_{2.5}Br_{0.5}$. Such a large energy disparity between the perovskite and PbI_2 would form a barrier for charge injection of the holes from $CsPbI_{2.5}Br_{0.5}$ into PbI_2 and thus should not behave as the bridge for intergrain carrier transport. Therefore, the carrier blocking effect of PbI_2 between perovskite grains is conducive to the extraction and collection of charge carriers generated in the perovskite grains by the charge transporting layers, leading to reduced charge recombination in passivated devices.

Having confirmed the influences of incorporation of excess PbI_2 on the device performance, crystal quality, and optoelectronic properties, we further investigated the device physics to gain better insight into the passivation effects in charge transport kinetics. As illustrated in **Figure 4**a, the light-dependent V_{OC} results present the corresponding slope of 1.76 K_BT/q for the 1.02 PbI_2-based device, which is smaller than that of control device (2.48K_BT/q). In general, the deviation in slope from the value of K_BT/q to $2K_BT/q$ indicates the trap-assisted Shockley–Read–Hall dominants in device.[63] The reduced slope indicates that trap-assisted charge recombination process is effectively suppressed through the inclusion of excess PbI_2. The light-dependent J_{SC} ($J_{SC} \propto I^{\alpha}$) were also conducted and displayed in Figure S9 in the Supporting Information. The exponent α close to 1 indicates the fully suppressed space charge effect in a solar cell owing to the absence of interfacial barrier or carrier imbalance.[64,65] The 1.00 PbI_2-based device exhibits an $\alpha = 1.012$ with respect to an $\alpha = 1.001$ of the 1.02-PbI_2 device. This result suggests that the proper PbI_2 additive in precursor could effectively suppress the charge recombination and improve electron extraction capability from the perovskite layer, benefiting the charge collection inside the $CsPbI_{2.5}Br_{0.5}$ PSCs.

As mentioned earlier, the excess PbI_2 in $CsPbI_{2.5}Br_{0.5}$ perovskite films is closely related to the enhanced device performance, especially for the improved V_{OC} and FF. A series of device characterizations were then carried out for the detailed understand of such improvements. The charge-recombination lifetime and charge-extraction time of the $CsPbI_{2.5}Br_{0.5}$ PSCs with different amount of PbI_2 were compared based on transient photovoltage (TPV) and transient photocurrent (TPC) measurements (Figure 4b,c). We observe a longer charge-recombination lifetime (7.00 µs) and shorter charge-extraction time (0.77 µs) for the 1.02-PbI_2 device, while those of the 1.00-PbI_2 device are 3.81 and 1.85 µs, respectively. The results indicate that the excess PbI_2 could suppress charge recombination and enhance extraction efficiency owing to the enhanced crystallinity and reduced trap states, benefiting the improvements of device parameters.

The transport and recombination resistances within different devices were further extracted from the Nyquist plots of the electrochemical impedance spectra (EIS), as shown in Figure 4d.[66,67] The Nyquist plots typically can be demarked into two main regions: at low and high frequencies. Normally, the low-frequency region represents the recombination

© 2020 The Authors. Published by WILEY-VCH Verlag GmbH & Co. KGaA, Weinheim

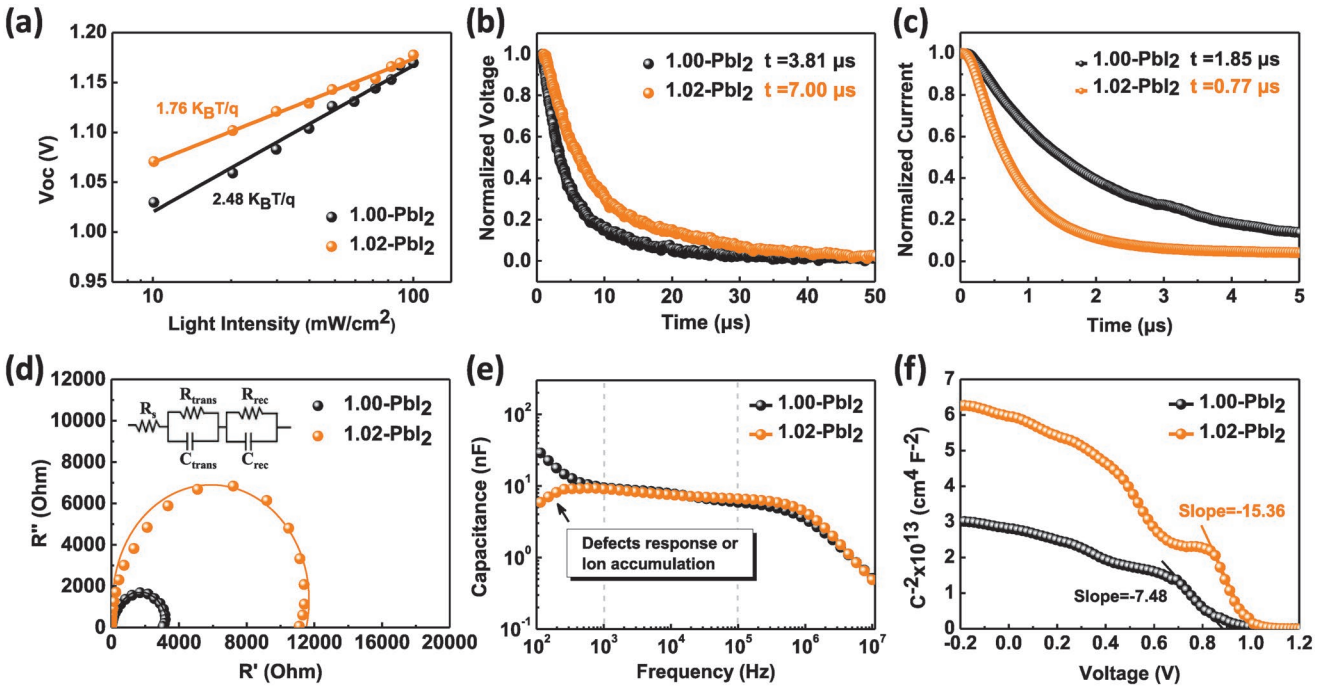

Figure 4. a) Light intensity dependent *J*–*V* measurements of inorganic $CsPbI_{2.5}Br_{0.5}$ PSCs fabricated from 1.00-PbI_2 and 1.02-PbI_2 perovskite precursors. b) TPV measurements, c) TPC measurements, and d) Nyquist plots from EIS for inorganic $CsPbI_{2.5}Br_{0.5}$ PSCs fabricated from 1.00-PbI_2 and 1.02-PbI_2 perovskite precursors. e) Frequency-dependent capacitance of the devices measured under dark at room temperature. f) Mott–Schottky (MS) plots of the PSCs with 1.00- and 1.02-PbI_2.

process, including recombination chemical capacitance (C_{rec}) and the recombination resistance (R_{rec}). The high-frequency region represents the transport process, including the transport chemical capacitance (C_{trans}) and the transport resistance (R_{trans}).[68] The detailed parameters are shown in Table S3 in the Supporting Information. By contrast, the extracted R_{trans} values decrease from 53.8 to 33.4 Ω for the control and 1.02-PbI_2 devices, respectively, accompanied with an increase in the R_{rec} from 3200 to 11 300 Ω. The decreased R_{trans} and increased R_{rec} indicate that the enhanced charge transport properties and effectively suppressed recombination rate are achieved in the PbI_2-passivation case. In addition, frequency-dependent capacitance under dark condition was obtained, as shown in Figure 4e. The capacitance plateau in middle frequency (10^3–10^5 Hz) is known as a result of electric polarization, caused by dipole polarization or geometrical capacitance of the perovskite. Whereas the capacitance in low frequency (<10^3 Hz) is due to electrode polarization, which is in relation to the defect response or ion accumulation in the perovskite.[11,69] According to the profiles, the control and 1.02-PbI_2 devices present the same capacitance plateaus (≈10 nF) in middle frequency, suggesting the same perovskite geometrical capacitance. However, the higher defect density in the 1.00-PbI_2 film leads to the much larger capacitance in low frequency in contrast to the 1.02-PbI_2 sample, which is believed to ensure the long-term operational stability of devices under illumination.

We experimentally confirmed the synergetic improvements from PbI_2-passivation in trap density, charge separation, and transfer. Finally, the effect of excess PbI_2 on the built-in potential was then investigated by capacitance–voltage (*C*–*V*) measurements. Figure 4f gives the Mott–Schottky (MS) plots $1/C^2$ versus voltage obtained from the *C*–*V* measurements. The relationship between the capacitance and bias voltage can be summarized by the Mott–Schottky Equation (2)[24]

$$\frac{1}{C^2} = \frac{2}{A^2 q \varepsilon_r \varepsilon_0 N}\left(V_{bi} - V - \frac{2kT}{q}\right) \quad (2)$$

where *C* is the capacitance under applied voltage (V), V_{bi} is the built-in potential at equilibrium, *q* is the elemental charge (1.60×10^{-19} C), *A* is the active area, ε_r is the relative permittivity (= 35), ε_0 is the vacuum permittivity (8.85×10^{-12} F m^{-1}), and N is the carrier concentration. From Equation (2), the slope gives the carrier concentration of the device ($-2/q\varepsilon N$).[24] Based on the results, the slope of the 1.02-PbI_2 device (–15.36) exhibits an over twofold increase with respect to the control device (–7.48), illustrating the much enhanced charge extraction and lower charge density within the perovskite film due to the passivation of PbI_2. Moreover, V_{bi} extracted from the intercepts of the linear region with the X-axis[70] shows a similar trend with the V_{OC} values from the *J*–*V* curves. The relatively higher V_{bi} of the 1.02-PbI_2 PSCs indicates the increased driving force for the separation of photogenerated carriers and the efficient suppression of electron–hole recombination, which is attributed to the improved V_{OC} and FF.

Furthermore, we tested the electroluminescence (EL) spectra of the devices, operating as light-emitting diodes (LEDs) in the dark and under the forward voltage bias. Obviously, both devices show the visible EL and a same emission peak located at 680 nm (Figure S10, Supporting Information). Meanwhile,

© 2020 The Authors. Published by WILEY-VCH Verlag GmbH & Co. KGaA, Weinheim

the 1.02-PbI_2 device displays a stronger EL intensity, further indicating the nonradiative losses in the perovskite layer have been significantly suppressed by PbI_2 passivation.

4. Conclusion

In summary, we systematically studied the influences of PbI_2-passivation in mixed-halide $CsPbI_{2.5}Br_{0.5}$ PSCs. The morphology and structural characterizations highlight the negligible influence of the excess PbI_2 on the final phase composition, while the induced effect of the PbI_2 additive significantly regulates the nucleation process and produces the high-quality perovskite film with improved grain sizes and crystallinity. The residual PbI_2 at the GBs could serve as a passivator, greatly passivating the trap state, reducing the carrier recombination loss, inhibiting ion segregation. Moreover, the carrier blocking effect of PbI_2 between perovskite grains facilitates the extraction and collection of charge carriers by the charge transporting layers and thus the reduced charge recombination. As a result, the optimized $CsPbI_{2.5}Br_{0.5}$ PSCs delivered an excellent PCE of 17.1% with a high open-circuit voltage of 1.25 V, in which the V_{OC}-deficits reduce to 0.57 V. More importantly, an excellent operational stability was observed for the mixed-halide $CsPbI_{2.5}Br_{0.5}$ PSCs with excess PbI_2 decoration, which 1.02-PbI_2 device maintains 76% of its initial efficiency after continuous power output at the MPP for 420 h under continuous illumination. This is the first report that achieves the long-term operational stability of the $CsPbI_xBr_{3-x}$ PSCs under continuous illumination at the MPP. Our findings show that composition engineering is an effective strategy to improve all-inorganic PSCs and provide important insights to further improve the efficiency and operational stability of all-inorganic PSCs and perovskite optoelectronic devices.

5. Experimental Section

Materials: Lead iodide (PbI_2, 99.99%) was purchased from TCI (Shanghai) Development Co., Ltd.. Cesium bromide (CsBr, 99.999%), cesium iodide (CsI, 99.999%), DMF (>99.0%), and DMSO was purchased from Sigma-Adrich. SnO_2 colloid (tin (IV) oxide (15%), CAS No. 18282-10-5) precursor was purchased from Alfa Aesar. Ethanol (99.5%) and zinc acetate dihydrate (>98%) were purchased from Acros. Potassium hydroxide (KOH, 87%) was purchased from Merck. 1-Butanol (>99.5%) was purchased from Rich Joint. ZnO nanoparticles were synthesized based on the procedure reported by Janssen and co-workers.[71] Spiro-OMeTAD (99.8%), 4-*tert*-butylpyridine (tBP), tris(2-(1*H*-pyrazol-1-yl)-4-*tert*-butylpyridine)cobalt(III)-tris(bis(trifluoromethylsulfonyl)imide) (FK209), and bis(trifluoromethylsulfonyl)amine lithium salt (Li-TFSI) were purchased from Xi'an Polymer Light Technology Corp., China. All materials were used without further purification.

PSCs Fabrication: Glass/ITO substrates were cleaned by successive sonication in deionized water, detergent, and isopropanol for 30 min each and then dried in an oven. The glass/ITO substrates were treated under oxygen plasma for 4 min before use. The SnO_2 layer was prepared by spin-coating the diluted SnO_2 colloid precursor with deionized (DI) water (1:6.5) onto ITO substrates at 3000 rpm for 30 s. The ZnO nanoparticles (5 mg mL^{-1}) were spun coated onto ITO/SnO_2 substrates at 2500 rpm for 30 s, followed by thermal annealing in air at 150 °C for 30 min. The perovskite precursor solution was prepared by dissolving x mmol PbI_2 (x = 1.00, 1.02, 1.04, 1.06), 0.5 mmol CsBr, and 0.5 mmol CsI in a mixture of DMSO and DMF (9:1 v/v) (1 mL) and stirred overnight in a glovebox. The perovskite precursor solution was spun onto ITO/SnO_2/ZnO substrates at 1500 rpm for 15 s and 5000 rpm for 30 s. Subsequently, the substrates were thermally annealed by a two-step annealing process at 45 °C for 60 s and 300 °C for 60 s. The Spiro-OMeTAD HTL was spun on the perovskite film at 4000 rpm for 30 s, which was prepared by dissolving 72.3 mg Spiro-OMeTAD, 28.8 µL of tBP, and 17.5 µL of a LiTFSI stock solution (520 mg mL^{-1} in acetonitrile) and 29 µL of an FK209 stock solution (300 mg mL^{-1} in acetonitrile) in 1 mL chlorobenzene. Finally, a 12 nm MoO_3 and 100 nm silver (Ag) were thermally evaporated under vacuum, respectively. A nonrefractive mask was employed to determine the effective device area of 0.04 cm^2.

PSCs Characterization: The current density–voltage (J–V) characteristics were measured under a computer controlled Keithley 2400 sourcemeter under 1 sun, AM 1.5G solar simulator (Taiwan, Enlitech SS-F5). The light intensity at each wavelength was calibrated by a standard silicon solar cell (certified by National Renewable Energy Laboratory) before testing, giving a value of 100 mW cm^{-2}. The EQE spectra were performed on a commercial EQE measurement system (Taiwan, Enlitech, QE-R). The UV–vis absorption spectra were recorded on an HP 8453E spectrophotometer. The bandgap (E_g) was estimated by using UV–vis absorption spectrum and the equation $(Ahv/K)^2 = hv - E_g$. The VBMs of perovskite and PbI_2 films were measured by photoelectron yield spectra (AC-3). The CBMs were calculated by $E_{CBM} = E_g + E_{VBM}$. The SEM images were obtained with a Hitachi FE-SEM S-4800 field emission scanning electron microscope (Japan) based on the sample structure of ITO/SnO_2/ZnO/perovskite. Based on the data acquired in the range of 10°–60° in θ to 2θ mode, the perovskite crystal structure was investigated using an X-ray diffraction (PANalytical X'pert PRO) equipped with a Cu-K_α X-ray tube, using ITO/SnO_2/ZnO/perovskite as samples. The PL spectra were recorded with an FLS920 spectrofluorometer (Edinburgh) and an HP 8453 spectrophotometer. The defect-state density was extracted by the dark current–voltage characteristics with an electron-only device with architecture of ITO/SnO_2/ZnO/perovskite/PCBM/Ag. TPV, TPC, EIS, and C–V measurements were carried out with a Paios 4.0 measurement instrument (FLUXiM AG, Switzerland). The EIS spectra were measured at an applied bias of V_{OC} with a frequency range from 10 MHz to 10 Hz and oscillating amplitude of 10 mV under illumination with white LED array (720 W m^{-2} integrated power). The EL measurement was recorded by a commercialized system (XPQY-EQE-350-1100, Guangzhou Xi Pu Optoelectronics Technology Co., Ltd.).

Supporting Information

Supporting Information is available from the Wiley Online Library or from the author.

Acknowledgements

J.T. and J.W. contributed equally to this work. The work was financially supported by the Ministry of Science and Technology (Nos. 2017YF0206600 and 2019YFA0705900), the Basic and Applied Basic Research Major Program of Guangdong Province (No. 2019B030302007), the Natural Science Foundation of China (Nos. 91733302 and 51803060), and the Science and Technology Program of Guangdong Province, China (No. 2018A030313045). N.L. gratefully acknowledges the financial support from the Deutsche Forschungsgemeinschaft (DFG) research grant: BR 4031/13-1. C.J.B. gratefully acknowledges the financial support through the "Aufbruch Bayern" initiative of the state of Bavaria (EnCN and SFF), the Bavarian Initiative "Solar Technologies go Hybrid" (SolTech), and the SFB 953 (DFG, Project No. 182849149).

Conflict of Interest

The authors declare no conflict of interest.

© 2020 The Authors. Published by WILEY-VCH Verlag GmbH & Co. KGaA, Weinheim

Keywords

composition engineering, $CsPbI_{2.5}Br_{0.5}$, defect passivation, operationally stable, PbI_2

Received: February 24, 2020
Revised: March 31, 2020
Published online: June 2, 2020

[1] C. C. Stoumpos, C. D. Malliakas, M. G. Kanatzidis, *Inorg. Chem.* **2013**, *52*, 9019.
[2] H. J. Snaith, *J. Phys. Chem. Lett.* **2013**, *4*, 3623.
[3] J. H. Noh, S. H. Im, J. H. Heo, T. N. Mandal, S. I. Seok, *Nano Lett.* **2013**, *13*, 1764.
[4] F. Hao, C. C. Stoumpos, R. P. H. Chang, M. G. Kanatzidis, *J. Am. Chem. Soc.* **2014**, *136*, 8094.
[5] C. Wang, J. Hu, C. Li, S. Qiu, X. Liu, L. Zeng, C. Liu, Y. Mai, F. Guo, *Sol. RRL* **2020**, *4*, 1900389.
[6] L. Zeng, Z. Chen, S. Qiu, J. Hu, C. Li, X. Liu, G. Liang, C. J. Brabec, Y. Mai, F. Guo, *Nano Energy* **2019**, *66*, 104099.
[7] I. Zarazua, G. Han, P. P. Boix, S. Mhaisalkar, F. Fabregat-Santiago, I. Mora-Sero, J. Bisquert, G. Garcia-Belmonte, *J. Phys. Chem. Lett.* **2016**, *7*, 5105.
[8] K. O. Brinkmann, J. Zhao, N. Pourdavoud, T. Becker, T. Hu, S. Olthof, K. Meerholz, L. Hoffmann, T. Gahlmann, R. Heiderhoff, M. F. Oszajca, N. A. Luechinger, D. Rogalla, Y. Chen, B. Cheng, T. Riedl, *Nat. Commun.* **2017**, *8*, 13938.
[9] S. Chen, X. Wen, S. Huang, F. Huang, Y.-B. Cheng, M. Green, A. Ho-Baillie, *Sol. RRL* **2017**, *1*, 1600001.
[10] J. Wang, J. Zhang, Y. Zhou, H. Liu, Q. Xue, X. Li, C. C. Chueh, H. L. Yip, Z. Zhu, A. K. Y. Jen, *Nat. Commun.* **2020**, *11*, 177.
[11] G. E. Eperon, S. D. Stranks, C. Menelaou, M. B. Johnston, L. M. Herz, H. J. Snaith, *Energy Environ. Sci.* **2014**, *7*, 982.
[12] R. J. Sutton, G. E. Eperon, L. Miranda, E. S. Parrott, B. A. Kamino, J. B. Patel, M. T. Hörantner, M. B. Johnston, A. A. Haghighirad, D. T. Moore, H. J. Snaith, *Adv. Energy Mater.* **2016**, *6*, 1502458.
[13] Z. Li, M. Yang, J.-S. Park, S.-H. Wei, J. J. Berry, K. Zhu, *Chem. Mater.* **2016**, *28*, 284.
[14] W. Ahmad, J. Khan, G. Niu, J. Tang, *Sol. RRL* **2017**, *1*, 1700048.
[15] P. Wang, X. Zhang, Y. Zhou, Q. Jiang, Q. Ye, Z. Chu, X. Li, X. Yang, Z. Yin, J. You, *Nat. Commun.* **2018**, *9*, 2225.
[16] G. E. Eperon, G. M. Paternò, R. J. Sutton, A. Zampetti, A. A. Haghighirad, F. Cacialli, H. J. Snaith, *J. Mater. Chem. A* **2015**, *3*, 19688.
[17] Q. Wang, X. Zheng, Y. Deng, J. Zhao, Z. Chen, J. Huang, *Joule* **2017**, *1*, 371.
[18] B. Li, Y. Zhang, L. Fu, T. Yu, S. Zhou, L. Zhang, L. Yin, *Nat. Commun.* **2018**, *9*, 1076.
[19] K. Wang, Z. Jin, L. Liang, H. Bian, H. Wang, J. Feng, Q. Wang, S. Liu, *Nano Energy* **2019**, *58*, 175.
[20] J. Xie, P. Hang, H. Wang, S. Zhao, G. Li, Y. Fang, F. Liu, X. Guo, H. Zhu, X. Lu, X. Yu, C. C. S. Chan, K. S. Wong, D. Yang, J. Xu, K. Yan, *Adv. Mater.* **2019**,*31*, 1902543.
[21] W. Meng, Y. Hou, A. Karl, E. Gu, X. Tang, A. Osvet, K. Zhang, Y. Zhao, X. Du, J. G. Cerrillo, N. Li, C. J. Brabec, *ACS Energy Lett.* **2020**, *5*, 271.
[22] Y. Wang, X. Liu, T. Zhang, X. Wang, M. Kan, J. Shi, Y. Zhao, *Angew. Chem., Int. Ed.* **2019**, *58*, 16691.
[23] Y. Wang, T. Zhang, M. Kan, Y. Li, T. Wang, Y. Zhao, *Joule* **2018**, *2*, 2065.
[24] Y. Wang, T. Zhang, M. Kan, Y. Zhao, *J. Am. Chem. Soc.* **2018**, *140*, 12345.
[25] K. Wang, Z. Jin, L. Liang, H. Bian, D. Bai, H. Wang, J. Zhang, Q. Wang, S. Liu, *Nat. Commun.* **2018**, *9*, 4544.
[26] J. Yuan, X. Ling, D. Yang, F. Li, S. Zhou, J. Shi, Y. Qian, J. Hu, Y. Sun, Y. Yang, X. Gao, S. Duhm, Q. Zhang, W. Ma, *Joule* **2018**, *2*, 2450.
[27] S. Dastidar, D. A. Egger, L. Z. Tan, S. B. Cromer, A. D. Dillon, S. Liu, L. Kronik, A. M. Rappe, A. T. Fafarman, *Nano Lett.* **2016**, *16*, 3563.
[28] C. F. J. Lau, X. Deng, J. Zheng, J. Kim, Z. Zhang, M. Zhang, J. Bing, B. Wilkinson, L. Hu, R. Patterson, S. Huanga, A. Ho-Baillie, *J. Mater. Chem. A* **2018**, *6*, 5580.
[29] S. Xiang, W. Li, Y. Wei, J. Liu, H. Liu, L. Zhu, S. Yang, H. Chen, *iScience* **2019**, *15*, 156.
[30] S. Xiang, W. Li, Y. Wei, J. Liu, H. Liu, L. Zhu, H. Chen, *Nanoscale* **2018**, *10*, 9996.
[31] Y. Jiang, J. Yuan, Y. Ni, J. Yang, Y. Wang, T. Jiu, M. Yuan, J. Chen, *Joule* **2018**, *2*, 1356.
[32] T. Zhang, M. I. Dar, G. Li, F. Xu, N. Guo, M. Grätzel, Y. Zhao, *Sci. Adv.* **2017**, *3*, e1700841.
[33] A. Swarnkar, A. R. Marshall, E. M. Sanehira, B. D. Chernomordik, D. T. Moore, J. A. Christians, T. Chakrabarti, J. M. Luther, *Science* **2016**, *354*, 92.
[34] Q. Ye, Y. Zhao, S. Mu, F. Ma, F. Gao, Z. Chu, Z. Yin, P. Gao, X. Zhang, J. You, *Adv. Mater.* **2019**, *31*, 1905143.
[35] X. Jia, C. Zuo, S. Tao, K. Sun, Y. Zhao, S. Yang, M. Cheng, M. Wang, Y. Yuan, J. Yang, F. Gao, G. Xing, Z. Wei, L. Zhang, H.-L. Yip, M. Liu, Q. Shen, L. Yin, L. Han, S. Liu, L. Wang, J. Luo, H. Tan, Z. Jin, L. Ding, *Sci. Bull.* **2019**, *64*, 1532.
[36] C. Chien-Yu, L. Hung-Yu, C. Kai-Ming, T. Wei-Lun, H. Yu-Ching, T. Cheng-Si, L. Hao-Wu, *Adv. Mater.* **2017**, *29*, 1605290.
[37] E. T. Hoke, D. J. Slotcavage, E. R. Dohner, A. R. Bowring, H. I. Karunadasa, M. D. McGehee, *Chem. Sci.* **2015**, *6*, 613.
[38] D. J. Slotcavage, H. I. Karunadasa, M. D. McGehee, *ACS Energy Lett.* **2016**, *1*, 1199.
[39] K. Domanski, E. A. Alharbi, A. Hagfeldt, M. Grätzel, W. Tress, *Nat. Energy* **2018**, *3*, 61.
[40] L. Meng, J. You, Y. Yang, *Nat. Commun.* **2018**, *9*, 5265.
[41] M. V. Khenkin, K. M. Anoop, E. A. Katz, I. Visoly-Fisher, *Energy Environ. Sci.* **2019**, *12*, 550.
[42] Y. C. Kim, N. J. Jeon, J. H. Noh, W. S. Yang, J. Seo, J. S. Yun, A. Ho-Baillie, S. Huang, M. A. Green, J. Seidel, T. K. Ahn, S. I. Seok, *Adv. Energy Mater.* **2016**, *6*, 1502104.
[43] C. Eames, J. M. Frost, P. R. F. Barnes, B. C. O'Regan, A. Walsh, M. S. Islam, *Nat. Commun.* **2015**, *6*, 7497.
[44] S. J. Yoon, M. Kuno, P. V. Kamat, *ACS Energy Lett.* **2017**, *2*, 1507.
[45] J. M. Ball, A. Petrozza, *Nat. Energy* **2016**, *1*, 16149.
[46] Q. Chen, H. Zhou, T. B. Song, S. Luo, Z. Hong, H. S. Duan, L. Dou, Y. Liu, Y. Yang, *Nano Lett.* **2014**, *14*, 4158.
[47] L. Wang, C. McCleese, A. Kovalsky, Y. Zhao, C. Burda, *J. Am. Chem. Soc.* **2014**, *136*, 12205.
[48] B. W. Park, N. Kedem, M. Kulbak, D. Y. Lee, W. S. Yang, N. J. Jeon, J. Seo, G. Kim, K. J. Kim, T. J. Shin, G. Hodes, D. Cahen, S. Il Seok, *Nat. Commun.* **2018**, *9*, 3301.
[49] Y. Yu, C. Wang, C. R. Grice, N. Shrestha, D. Zhao, W. Liao, L. Guan, R. A. Awni, W. Meng, A. J. Cimaroli, K. Zhu, R. J. Ellingson, Y. Yan, *ACS Energy Lett.* **2017**, *2*, 1177.
[50] T. Niu, J. Lu, M. Tang, D. Barrit, D.-M. Smilgies, Z. Yang, J. Li, Y. Fan, T. Luo, I. McCulloch, A. Amassian, S. Liu, K. Zhao, *Energy Environ. Sci.* **2018**, *11*, 3358.
[51] E. Mosconi, G. Grancini, C. Roldán-Carmona, P. Gratia, I. Zimmermann, M. K. Nazeeruddin, F. D. Angelis, *Chem. Mater.* **2016**, *28*, 3612.
[52] C. Roldán-Carmona, P. Gratia, I. Zimmermann, G. Grancini, P. Gao, M. Graetzelb, M. K. Nazeeruddin, *Energy Environ. Sci.* **2015**, *8*, 3550.
[53] H. Tan, A. Jain, O. Voznyy, X. Lan, F. P. García de Arquer, J. Z. Fan, R. Quintero-Bermudez, M. Yuan, B. Zhang, Y. Zhao, F. Fan, P. Li, L. Na Quan, Y. Zhao, Z.-H. Lu, Z. Yang, S. Hoogland, E. H. Sargent, *Science* **2017**, *355*, 722.

© 2020 The Authors. Published by WILEY-VCH Verlag GmbH & Co. KGaA, Weinheim

[54] Q. Jiang, Z. Chu, P. Wang, X. Yang, H. Liu, Y. Wang, Z. Yin, J. Wu, X. Zhang, J. You, *Adv. Mater.* **2017**, *29*, 1703852.
[55] T. J. Jacobsson, J.-P. Correa-Baena, E. H. Anaraki, B. Philippe, S. D. Stranks, M. E. F. Bouduban, W. Tress, K. Schenk, J. Teuscher, J.-E. Moser, H. Rensmo, A. Hagfeldt, *J. Am. Chem. Soc.* **2016**, *138*, 10331.
[56] J. Euvrard, O. Gunawan, D. B. Mitzi, *Adv. Energy Mater.* **2019**, *9*, 1902706.
[57] G. Yin, H. Zhao, H. Jiang, S. Yuan, T. Niu, K. Zhao, Z. Liu, S. Liu, *Adv. Funct. Mater.* **2018**, *28*, 1803269.
[58] W. S. Yang, J. H. Noh, N. J. Jeon, Y. C. Kim, S. Ryu, J. Seo, S. Il Seok, *Science* **2015**, *348*, 1234.
[59] Y. Wu, A. Islama, X. Yang, C. Qin, J. Liu, K. Zhang, W. Penga, L. Han, *Energy Environ. Sci.* **2014**, *7*, 2934.
[60] Q. Lin, A. Armin, R. C. R. Nagiri, P. L. Burn, P. Meredith, *Nat. Photonics* **2015**, *9*, 106.
[61] W. Li, C. Zhang, Y. Ma, C. Liu, J. Fan, Y. Mai, R. E. I. Schropp, *Energy Environ. Sci.* **2018**, *11*, 286.
[62] T. Niu, J. Lu, R. Munir, J. Li, D. Barrit, X. Zhang, H. Hu, Z. Yang, A. Amassian, K. Zhao, S. Liu, *Adv. Mater.* **2018**, *30*, 1706576.
[63] M. Bernechea, N. C. Miller, G. Xercavins, D. So, A. Stavrinadis, G. Konstantatos, *Nat. Photonics* **2016**, *10*, 521.
[64] L. J. A. Koster, V. D. Mihailetchi, H. Xie, P. W. M. Blom, *Appl. Phys. Lett.* **2005**, *87*, 203502.
[65] A. K. K. Kyaw, D. H. Wang, V. Gupta, W. L. Leong, L. Ke, G. C. Bazan, A. J. Heeger, *ACS Nano* **2013**, *7*, 4569.
[66] Z. Zhu, Y. Bai, H. K. H. Lee, C. Mu, T. Zhang, L. Zhang, J. Wang, H. Yan, S. K. So, S. Yang, *Adv. Funct. Mater.* **2014**, *24*, 7357.
[67] J. A. Christians, R. C. M. Fung, P. V. Kamat, *J. Am. Chem. Soc.* **2014**, *136*, 758.
[68] J. Tian, Q. Xue, X. Tang, Y. Chen, N. Li, Z. Hu, T. Shi, X. Wang, F. Huang, C. J. Brabec, H. L. Yip, Y. Cao, *Adv. Mater.* **2019**, *31*, 1901152.
[69] H. S. Kim, I. H. Jang, N. Ahn, M. Choi, A. Guerrero, J. Bisquert, N. G. Park, *J. Phys. Chem. Lett.* **2015**, *6*, 4633.
[70] C. Chen, Y. Xu, S. Wu, S. Zhang, Z. Yang, W. Zhang, H. Zhu, Z. Xiong, W. Chen, W. Chen, *J. Mater. Chem. A* **2018**, *6*, 7903.
[71] W. J. E. Beek, M. M. Wienk, M. Kemerink, X. Yang, R. A. J. Janssen, *J. Phys. Chem. B* **2005**, *109*, 9505.

© 2020 The Authors. Published by WILEY-VCH Verlag GmbH & Co. KGaA, Weinheim